

# Few-shot Segmentation with Optimal Transport Matching and Message Flow

Weide Liu, Chi Zhang, Henghui Ding, Tzu-Yi Hung and Guosheng Lin

**Abstract**—We address the challenging task of few-shot segmentation in this work. It is essential for few-shot semantic segmentation to fully utilize the support information. Previous methods typically adapt masked average pooling over the support feature to extract the support clues as a global vector, usually dominated by the salient part and loses some important clues. In this work, we argue that every support pixel’s information is desired to be transferred to all query pixels and propose a Correspondence Matching Network (CMNet) with an Optimal Transport Matching module to mine out the correspondence between the query and support images. Besides, it is important to fully utilize both local and global information from the annotated support images. To this end, we propose a Message Flow module to propagate the message along the inner-flow within the same image and cross-flow between support and query images, which greatly help enhance the local feature representations. We further address the few-shot segmentation as a multi-task learning problem to alleviate the domain gap issue between different datasets. Experiments on PASCAL VOC 2012, MS COCO, and FSS-1000 datasets show that our network achieves new state-of-the-art few-shot segmentation performance.

**Index Terms**—Few-shot Learning, Segmentation, Correspondence Matching Network, CMNet, Optimal Transport Matching, Message Flow

## I. INTRODUCTION

**S**EMANTIC segmentation is a fundamental task to assign every pixel with a label. With the rapid development of deep learning, fully supervised semantic segmentation has made significant improvements in recent years. One of the intrinsic limitations of the fully supervised segmentation is that it needs large amounts of annotated images to train the model. Another limitation is that the performance will drop very quickly when predicting unseen classes.

To address the above issues, few-shot segmentation is proposed to learn a network that can predict novel classes with only a few annotated data. Few-shot segmentation divides the data into support sets and query sets. The goal is to predict a binary mask in query images. The categories provided by the

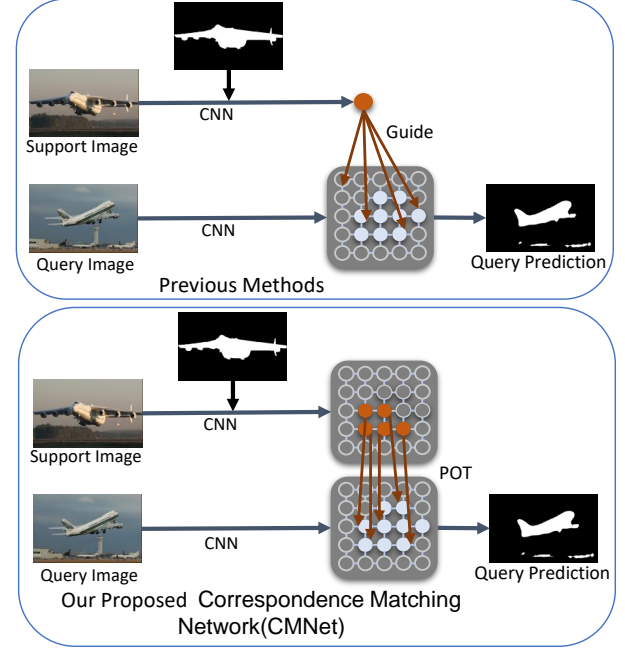


Fig. 1: Comparison between the pipeline of our proposed network with the previous methods of few-shot segmentation. Previous works (upper part) average the support features to a global vector to guide the query image’s predictions. In contrast, ours proposed CMNet (lower part) guides each query feature with specific clues by applying a partial optimal transport matching (POT) between query and support features.

annotated support sets should be predicted as foreground. Two-branch network architecture has been widely used [1]–[3] to pass the information between the query and support images. However, previous methods typically adapt masked average pooling over the support feature to extract the support clues as a global vector, usually dominated by the salient part and loses some important clues. Besides, the pixel relations between the image pair are unclear with only a global vector. As shown in Figure 2, previous methods [1], [2] simplify the many-to-many problem to the many-to-one problem by averaging the support features to a global vector to guide the query image’s predictions. In this way, every position for the query image will have the same clue. However, one obvious limitation is that it breaks the spatial structures and only captures the most dominant features on support images, resulting in limited parts of the support images being used to match the query images. We argue that every support pixel’s information is desired to

W. Liu is with School of Computer Science and Engineering, Nanyang Technological University (NTU), Singapore 639798 (e-mail: weide001@e.ntu.edu.sg).

C. Zhang is with School of Computer Science and Engineering, Nanyang Technological University (NTU), Singapore 639798 (e-mail: chi007@e.ntu.edu.sg).

H. Ding is with School of Electrical and Electronic Engineering, Nanyang Technological University (NTU), Singapore 639798 (e-mail: ding0093@e.ntu.edu.sg).

T. Hung is with Delta Research Center, Singapore (e-mail: tzuyi.hung@deltaww.com).

G. Lin is with School of Computer Science and Engineering, Nanyang Technological University (NTU), Singapore 639798 (e-mail: gslin@ntu.edu.sg).

Corresponding author: Guosheng Lin.

be transferred to all query pixels, yielding a many-to-many message problem [4].

PGNet [4] is a many-to-many work that proposes to transfer the information between the query set and support set with a structured representation by leveraging the pyramid graph connections. However, there are several limitations for such unconstrained many-to-many matching methods: 1) **Many-to-one matching.** A feature point from the query image may have more than one correspondence point in the support image, which results in that only the most discriminative parts of the query features connect to the support features [5]. 2) **Inappropriate matching.** The dominant parts in the query image connect too many points in the support image (including the dominant and the normal parts), which will result in inappropriate connections. For example, as shown in Figure 2, the bird's head features are connected to the body features. 3) **Unmatched parts.** Many query features may be unmatched due to the *many-to-one matching* problem. For example, as shown in Figure 2, most points from the support image match to the head of the bird in the query image; thus, most regions of the query image remain unmatched.

To mine out more correspondences between the query and support images and address the limitations of the previous graph network, we propose a constrained many-to-many matching method, partial optimal transport matching, to maximize the total correspondences between the query and support images. We fix the maximum matching flow at a value according to the object size obtained from the ground truth of the support image. This will stimulate the query feature to activate the object parts whose features are less discriminative but necessary to be matched. For example, we need to match the features between two birds in Figure 2. In the previous works, the most discriminative part *head* will be matched, but the remaining parts are not able to be matched. In contrast, our proposed optimal transport matching module could activate the less discriminative parts by setting a maximum matching flow based on the object size – if unmatched flows are detected, the query image is forced to activate the corresponding object parts and match them until no matching flow is left.

Furthermore, existing methods [1]–[3] concentrate more on global features while relatively overlook the information of the local feature representations. We spotlight the importance of the local representations for few shot segmentation tasks. To enhance the local feature representations, we develop a message flow module to propagate messages within one image (inner-flow) and between different images (cross-flow). We model the query and support features using graphs and propagate the information among them. The nodes are associated with local features, and the edges are associated with similarity information between nodes. Our optimal transport matching module also benefits from the enhanced local feature representations to generate the correspondences.

We tackle the few-shot segmentation task as a multi-task learning problem to handle the domain gap between different datasets. Previous works [1], [2], [4]–[10] use frozen backbones pretrained on ImageNet [11]. However, there are domain gaps between ImageNet and the target datasets. We find that multi-task learning will help the model recognize the new

objects and mitigate the data domain gap issue.

Our contributions are summarized as follows:

- We propose a partial optimal transport matching module, which is a constrained many-to-many matching method, for the few shot segmentation tasks. The query and support images are allowed to match more related areas as correspondences.
- We develop a message flow module to propagate the message between images along the inner-flow and cross-flow to enhance the local feature representations.
- We explore the few-shot segmentation task as a multi-task learning problem to alleviate the domain gap issue between different datasets.
- Experiments on PASCAL VOC 2012, MS COCO, FSS-1000 dataset show that our method outperforms the baseline and achieves new state-of-the-art performance.

## II. RELATED WORK

### A. Semantic Segmentation

Semantic segmentation is a fundamental computer vision task that aims to assign each pixel with a class label. Currently, the most popular architecture is fully convolutional networks (FCN) [12]. Which replaces the final fully-connected layer of conventional classification network with a  $1 \times 1$  convolutional layer and has been widely used in current state-of-the-art methods, included ours. Encoder-decoder [2], [13]–[31] is a popular structure used to reconstruct the high-resolution prediction map for semantic segmentation prediction. The encoder gradually downsamples the feature maps to obtain a large field-of-view, and the decoder recovers the fine-grained information. Dilated convolution [14] also aims to increase the field-of-view by increasing the convolution dilation without increase the parameters. In our network, we also follow the encoder-decoder structure with a dilated convolution for our semantic segmentation prediction.

### B. Few-shot Segmentation

Metric learning has been widely used in few-shot segmentation tasks. Such as CANet [1] uses the global feature from the support image to make a dense comparison to the query image. OSLSM [32] introduces a two-branch network consisting of support and query branches for few-shot segmentation, the support branch designed to guide the query set. CRNet [2] proposes that the query branch and the support branch can guide each other with a cross-reference mechanism. PL [33] employs the prototypical network for few-shot segmentation as metric learning. SG-One obtains a prototype vector from the support image to guide query prediction with a masked-average pooling. PANet [3] introduces a prototype alignment regularization between support and query images and guides each other.

Most of those metric learning for few-shot segmentation generate the prototype vector with global average pooling to guide the query image. However, such a strategy has two limitations: spatial information has been disregarded; another is that the objects' semantic information is underutilized. To

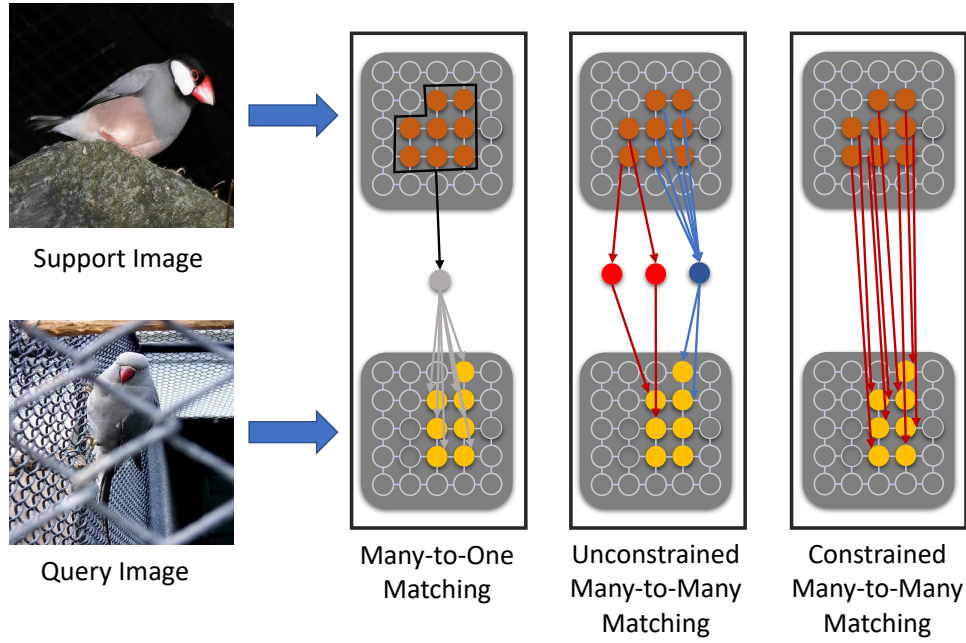


Fig. 2: Comparison between the different matching methods. Many-to-one matching methods average the support features to a global vector to guide the query image’s predictions, which results in an uncertain connection (grey line). The unconstrained many-to-many methods make the network attentive to the most discriminative parts (red lines indicate the accurate matching, blue lines indicate the inappropriate matching), making many query features unmatched. In contrast, our proposed constrained many-to-many matching method (optimal transport matching) encourages the network to mine more related correspondences.

fully use spatial information, we adopt the message flow module to propagate the local information between images to enhance the local feature representations.

### C. Optimal transport

Optimal transport provides a way to formulate the problem of transfer one distribution to another as linear programming, which can be solved by Sinkhorn algorithm [34]. Optimal transport has been widely used in many various computer vision tasks. Courty *et al.* [35] learns a transportation plan to step over the domain gap between the source domain to the target domain. Su *et al.* [36] matches the 3D shape with the optimal transport. Zhao *et al.* [37] employs a differential-optimal transport to tackle the visual tracking problem. In this paper, we use a partial optimal transport module to obtain the semantic correspondences between the query and support images. Few-shot segmentation task aims to predict binary masks to segment out the foreground objects in the testing image set with only a few annotated images. The categories in the training image set have no overlap with the testing image set. The annotated images are treated as support sets for the training and testing interface and provide the foreground categories to guide the segmentation of the unlabeled query set.

## III. METHODS

The critical technique for few-shot semantic segmentation is the way to propagate the local and global information

between the query and support images. Previous methods simply average the support feature to a global vector, serving as a general clue to guide every position of the query image. However, the global vector does not contain the information of spatial structures and only captures the most dominant information of the support features, which results in the limited parts of the support images being used to match the query images. The unconstrained many-to-many matching methods aim to address the problem with a weighted connection between each query and support features. However, due to the dominant feature problem, most of the feature points from the support image will match the most discriminative parts in the query image, which causes the remaining query features to be unmatched.

This section introduces a constrained many-to-many matching method to maximize the total correspondences between the query and support images to overcome the aforementioned flaws. Then we will introduce a message flow module to propagate messages within one image (inner-flow) and between different images (cross-flow) to enhance the local feature representations. Our optimal transport module also benefits from the enhanced local feature representations to generate the correspondences. Finally, we introduce how to tackle the few-shot segmentation task as a multi-task learning problem to handle the domain gap between different datasets.

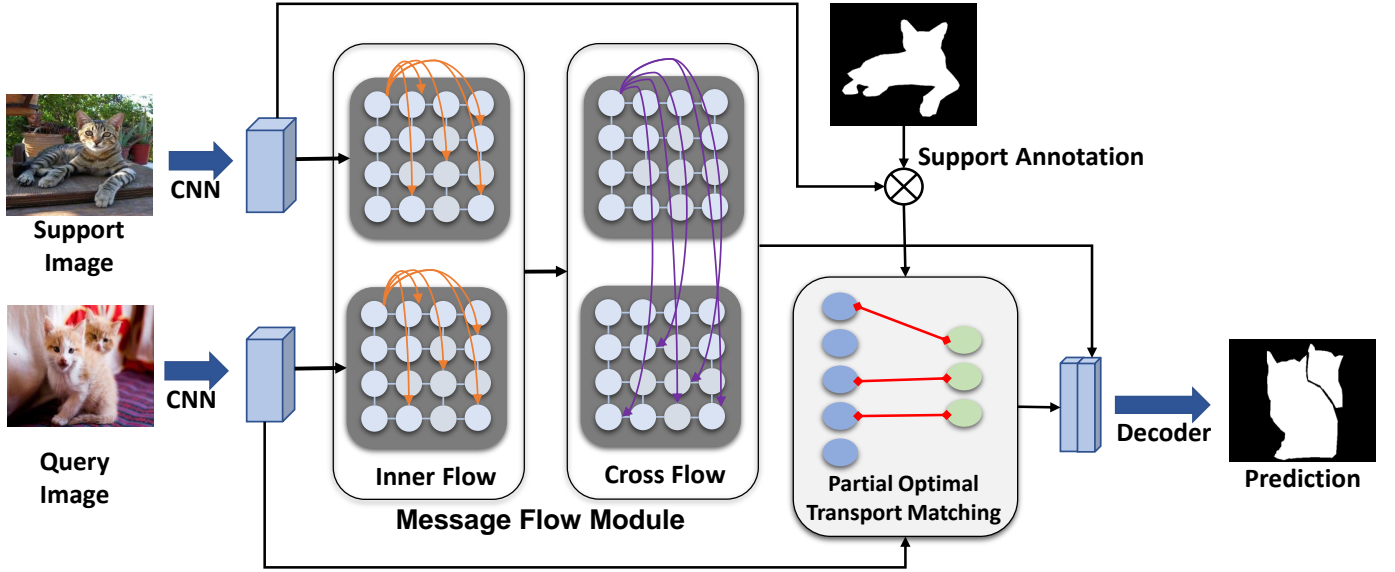


Fig. 3: Our network architecture. Our network mainly consists of a message flow module and a partial optimal matching module. We encode every support and query image pair into graphs with a shared-parameter CNN, then we propagate the message between the graph nodes using the inner-flow (inside one image) and cross-flow (across images) to enhance local features. Combined the optimal matching correspondences generated by our optimal matching module, we generate the query predictions with our decoder.

#### A. Partial Optimal Transport Module

**Optimal Transport.** Optimal transport aims to minimize the distance to transfer the source image distribution to the target distribution, which provides a way to generate the correspondence between two distributions. Specially, we treat the source distribution as the suppliers and the target as demanders. Support there are a set of suppliers  $\mathcal{S} = \{s_i | i = 1, 2, \dots, m\}$  required to transport goods to the demanders  $\mathcal{D} = \{d_j | j = 1, 2, \dots, k\}$ , and the cost per unit transport from each supplier to demander denotes  $c_{ij}$ . The goal of optimal transport is to cost as little as possible to transport as many goods as possible:

$$\text{minimize} \sum_{i,j}^m \sum_{j=1}^k c_{ij} x_{ij}. \quad (1)$$

where  $x_{ij}$  denotes the number of goods from  $s_i$  to  $d_j$ . Note that the total goods from the supplier should be equal to the demanders' demands, and the goal can be achieved by solving the linear programming problem.

**Partial Optimal Transport.** The total amount of goods provided by the supplier not always equal to the goods demanders required. To address this problem, partial optimal transport allows matching two asymmetric distribution with some absolute amount quantity, and we call this *absolute partial optimal transport*. In an absolute partial matching problem, the amount of weight-matched is defined as  $M$ , and the total transport flow will be equal to  $M$ :

$$\begin{aligned} x_{ij} &\geq 0, i = 1, \dots, m, j = 1, \dots, k \\ \sum_{j=1}^k x_{ij} &\leq w_i, i = 1, \dots, m \\ \sum_{i=1}^m x_{ij} &\leq u_j, j = 1, \dots, k \\ \sum_{i=1}^m \sum_{j=1}^k x_{ij} &= M \end{aligned} \quad (2)$$

where  $w_i$  denotes the number of goods the  $i_{th}$  supplier can provide and the  $u_j$  denotes the goods for  $j_{th}$  demander required. To achieve a partial matching goal, we treat this problem as a balanced transportation problem. Suppose total  $k$  demanders require  $w_d$  goods, while all the  $m$  suppliers can provide  $w_s$  goods (suppose  $w_d \geq w_s$ ), and a fixed amount of transport weight  $M \leq w_s$  is given. To balance the goods amount between supplier and demanders, we set a balanced flow  $M(\gamma) = w_d + w_s - M$ . Then we set a  $m + 1$  supplier as a dummy supplier to provide the supply a unbalanced weight  $M(\gamma) - w_s = w_d - M$  and a dummy demander  $k + 1$  to requires the unbalance demand weight  $M(\gamma) - w_d = w_s - M$ . Combine with the dummy supplier and demander, the balanced transportation problem can be solved as an optimal transport problem. We transfer the partial matching problem to a balanced transportation problem in the following way:

$$\begin{aligned} w_s &= \sum_{i=1}^m s_i, i = 1, \dots, m \\ w_d &= \sum_{j=1}^k d_j, j = 1, \dots, k \\ M(\gamma) &= w_d + w_s - M \\ w_{m+1} &= w_d - M \\ u_{k+1} &= w_s - M \\ c_{ij} &\geq 0 \\ c_{m+1,j} &= 0, j = 1, \dots, k \\ c_{i,k+1} &= 0, i = 1, \dots, m \\ c_{m+1,k+1} &= \infty. \end{aligned} \quad (3)$$

We set the dummy supplier's cost to dummy demander to  $\infty$  to prevent matching the dummy nodes. Then we set the cost from dummy supplier  $s_{m+1}$  to the normal demanders at zero



( $c_{m+1,j} = 0$ ), and the dummy demander  $d_{k+1}$  also no cost to match the remaining suppliers ( $c_{i,k+1} = 0$ ). Therefore, the normal suppliers will firstly provide  $w_s - M$  goods to the dummy demander and remain  $M$  goods to match the normal demanders. On the other hand, the normal demanders will receive  $wd - M$  goods from the dummy supplier as prior, and remain  $M$  goods will be provided by the normal suppliers. Therefore, only transport weight  $M$  will be matched with a nonzero cost between the normal suppliers and demanders. In this way, the partial optimal transport problem has been formulated as a balanced transportation problem to find the optimal flow from suppliers  $s_i, i = 1, 2..m$  to demanders  $s_j, j = 1, 2..k$ , which can be solved the same as the full optimal transport problem.

**Optimal Transport for Few-shot Segmentation.** Metric learning methods are widely used to tackle the few-shot segmentation task. CRNet and CANet generate a global support vector [1], [2] to find an optimal vector to **match** all the elements from the query set. However, those methods ignore the local discriminative representations from the support images. PANet [3] generates a cosine similarity map with local information as the final prediction, while PFENet [6] generates a prior mask by obtaining the pixel-wise correspondence from the cosine similarity maps.

Different from the previous works, our method not only takes the pixel-wise correspondence value from the cosine similarity maps as an intermediate representation; we also find the correspondences between the query and support images by solving a **many-to-many** matching problem.

In particular, we encode each image into features and model as a graph, each local representation denote as a node. The nodes from support images are set to suppliers  $s_i$  and set the query nodes as demanders  $d_j$ . The cost between suppliers and demanders depends on their cosine similarity:

$$c_{ij} = 1 - \frac{\mathbf{s}_i^T \mathbf{d}_j}{\|\mathbf{s}_i\| \|\mathbf{d}_j\|}. \quad (4)$$

In this way, we formulate the few-shot segmentation problem into a partial optimal matching problem as described above. By using the Sinkhorn algorithm [34], we obtain an optimal flow from query to support image. The flow weight from each query node to the support node represents the correspondence between the nodes. By multiplying the binary support annotation to the support nodes, we filter out the irrelevant correspondences from the query image to the support image. The foreground probability maps will be generated With the flitted correspondences, while the correspondences' weight can be considered the foreground probability. Finally, we fuse the foreground probability map as a coarse object region to guide the feature maps to segment the final query masks.

### B. Message Flow Module

Previous methods always concentrate on the global information of the objects while overlooking the local feature information. In this section, we develop a message flow module to enhance the local feature representations by propagating the messages within one image along inner-flow and between cross images along cross-flow.

TABLE I: Ablation experiments on the Message Flow Module (MFM), Multi-Task Learning, Mask-Refine (MR) module, Prior Mask (PM) and the Partial Optimize Transport module (POT). Every module brings performance improvement over the baseline model. The results reported on PASCAL VOC 2012 dataset with standard mIoU(%).

MFM	Multi-Task	MR	PM	POT	1-shot
					59.1
✓					60.2
✓	✓				61.0
✓	✓	✓			61.2
✓	✓	✓	✓		62.0
✓	✓	✓	✓	✓	62.5

TABLE II: Ablation experiments on the message flow module, The results reported on PASCAL VOC 2012 dataset with standard mIoU(%).

Method	mIoU
Baseline	59.1
Inner	59.7
Cross	59.9
Inner-Cross	60.2

We first employ a shared-parameter CNN to encode the images and model the feature maps as a graph: each node represents a local feature, and the edges are associated with the similarity between nodes. Every initial local feature first aggregates the contextual information by communicating to the connected nodes within the intra-image. Then the local information will be propagated to other images along the cross-flow.

**Positional Encoding.** Besides the object's visual appearance, we argue that the object's position cues can intuitively increase the object's distinctiveness. For example, the head always on top of the human, not the bottom, while the legs will be the bottom. Inspired by this, we integrate the visual and position information cues as our encoded features. To achieve this, we embed the spatial position information with a learnable spatial positional encoding [51]. Then we fuse the spatial position information and visual appearance features with:

$$f = f_a + P_{enc}(p_i). \quad (5)$$

Where  $f_a$  denotes the appearance features,  $P_{enc}$  denotes the positional encoding [51] and  $p_i$  denotes the position information.

**Inner and Cross-Flow Module.** Given a pair of graphs whose nodes are the local object features, we consider two kinds of graph message flow propagation [52], [53]; the inner-flow within the intra-image and cross-flow between the cross-images. We leverage the message passing formulation [54], [55] to pass on the flow's information.

In particular, we model both support and query image features generated with equation 5 to graphs. For every node

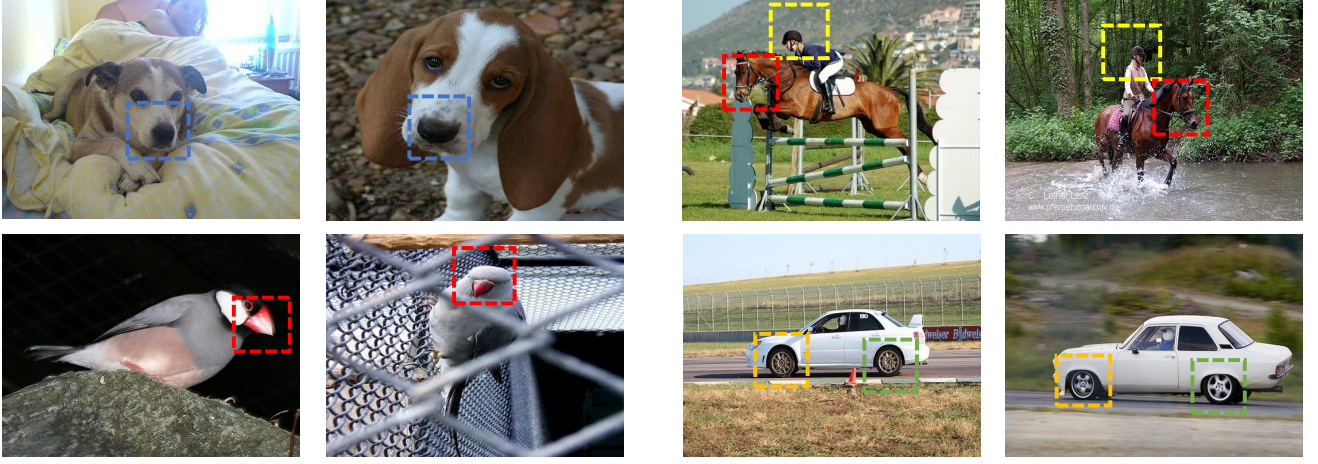


Fig. 4: Visualization of the partial optimal matching flows. Given two images (left and right), we plot the best matched patch of each local region.

TABLE III: Comparison our partial optimal transport module (Partial), full optimal transport (Full) module and the prior mask (PM). The results reported on PASCAL VOC 2012 dataset with standard mIoU(%).

Method	mIoU
Baseline	59.1
w/ Full	59.2
w/ Partial	59.5
w/ PM	60.2
w/ Full-PM	59.6
w/ Partial-PM	60.5

$q$  from the graphs, we aggregate all the message from its connected nodes and update information with a residual form:

$$f'_q = f_q + MLP(\text{concat}(f_q, m\mathcal{E} \rightarrow q)), \quad (6)$$

here *concat* denotes the concatenate operate on the channel dimension, MLP denotes the Multilayer Perceptron (MLP), which implements with  $1 \times 1$  convolution.  $m\mathcal{E} \rightarrow q$  denotes the aggregation message passing to the node  $q$  from its connected nodes, and  $f_q$  denotes the feature of the node  $q$ . For the inner-flow module, the connected nodes from its neighbor nodes and the cross-flow module connect the nodes between cross-images.

**Aggregation Message Passing.** We calculate the aggregation message  $m\mathcal{E} \rightarrow q$  with an attention mechanism. Inspired by [56], give a node feature  $\mathbf{q}_i$ , the keys  $\mathbf{k}_j$  and values  $\mathbf{v}_j$  from connected nodes, we generate the attention weight as graph edge weight:

$$\alpha_{i,j} = \text{SoftMax}(\mathbf{q}_i^T \mathbf{k}_j). \quad (7)$$

With the attention weight, we propagate the values from the connected nodes to the node  $q_i$  by aggregating the weighted value:

$$m_{\mathcal{E} \rightarrow q} = \sum_{j:(i,j) \in \mathcal{E}} \alpha_{i,j} \mathbf{v}_j. \quad (8)$$

We generate the node feature  $\mathbf{q}_i$ , the keys  $\mathbf{k}_j$  and values  $\mathbf{v}_j$  with a  $1 \times 1$  convolution from the query graph and the connected graph.

By propagating the message between nodes, we enhance the local feature representations, benefiting our optimal transport module and the final prediction.

### C. Multi-tasks training

Previous works [1], [2], [4]–[6], [38] always freeze the backbone pretrained from ImageNet [11], and train the remaining parameters. However, there exists a data domain gap between the ImageNet to target datasets, which hinders the model from recognizing the objects in the new domain. To solve this problem, we explore the few-shot segmentation task as a multi-task learning problem. In particular: 1) we first train a model in a fully supervised segmentation way with the training class data by removing all the images containing the validation classes. 2) After that, we replace the backbone parameter with the new parameter generated from step 1 and freeze it. 3) Finally, we fine-tune the remaining parameters the same as the standard few-shot segmentation training step [1], [2].

## IV. EXPERIMENT

### A. Experiment Setting

1) **Evaluation Metric:** Follow previous works [2], [32], we adopt the standard mean Intersection-Over-Union(mIoU) as our main evaluation metric. However, [33] also report their results with the mean of foreground IoU and background IoU (FBIoU), which ignore the categories. To be a fair comparison, we report our methods with both evaluation metrics.

The evaluation metrics are calculated as follows:

$$IoU = \frac{\text{Intersection}}{\text{Union}} = \frac{TP}{TP + FP + FN}, \quad (9)$$

$$mIoU = \frac{1}{n} \sum_{i=1}^n (IoU_n), \quad (10)$$

TABLE IV: Detailed 1-shot and 5-shot results in each split under the mIoU(%) evaluation metric with PASCAL VOC 2012 dataset. Our model outperforms all previous methods and achieves new state-of-the-art performance.

Method	1-shot					5-shot				
	split-0	split-1	split-2	split-3	mean	split-0	split-1	split-2	split-3	mean
FSS-1000 [38]	—	—	—	—	—	37.4	60.9	46.6	42.2	56.8
OSLSM [32]	33.6	55.3	40.9	33.5	40.8	35.9	58.1	42.7	39.1	43.9
co-FCN [39]	36.7	50.6	44.9	32.4	41.1	37.5	50.0	44.1	33.9	41.4
R-DFCN [40]	39.2	48.0	39.2	34.2	40.2	45.3	51.4	44.9	39.5	45.3
SG-One [41]	40.2	58.4	48.4	38.4	46.3	41.9	58.6	48.6	39.4	47.1
AMP [42]	41.9	50.2	46.7	34.7	43.4	41.8	55.5	50.3	39.9	46.9
Feat Weight [43]	47.0	59.6	52.6	48.3	51.9	50.9	62.9	56.5	50.1	55.1
PANet [3]	42.3	58.0	51.1	41.2	48.1	51.8	64.6	59.8	46.5	55.7
MDL [44]	39.7	58.3	46.7	36.3	45.3	40.6	58.5	47.7	36.6	45.9
OS <sub>Adv</sub> [45]	46.9	59.2	49.3	43.4	49.7	47.2	58.8	48.8	47.4	50.6
CANet [1]	52.5	65.9	51.3	51.9	55.4	55.5	67.8	51.9	53.2	57.1
CRNet [2]	56.8	65.8	49.4	50.6	55.7	58.7	67.9	54.2	53.5	58.8
RPMMS [46]	55.1	66.9	52.6	50.7	56.3	56.2	67.3	54.5	51.0	57.3
PPNet [47]	48.5	60.1	<b>55.7</b>	46.4	52.8	58.8	68.3	<b>66.7</b>	57.9	62.9
PFENet [6]	61.7	69.5	55.4	56.3	60.8	63.1	70.7	55.8	57.9	61.9
Ours	<b>65.4</b>	<b>71.5</b>	55.2	<b>58.1</b>	<b>62.5</b>	<b>67.0</b>	<b>71.7</b>	55.8	<b>59.9</b>	<b>63.6</b>

TABLE V: Detailed 1-shot and 5-shot results in each split under the mIoU(%) evaluation metric with pascal MS COCO dataset. Our model outperforms all previous methods and achieves new state-of-the-art performance.

Method	1-shot					5-shot				
	split-0	split-1	split-2	split-3	mean	split-0	split-1	split-2	split-3	mean
PANet [3]	—	—	—	—	20.9	—	—	—	—	29.7
FWB [43]	16.9	17.9	20.9	28.8	21.2	19.1	21.4	23.9	30.0	23.6
RPMMS [46]	29.5	<b>36.8</b>	28.9	27.0	30.5	33.8	<b>41.9</b>	32.9	33.3	35.5
PFENet [6]	34.3	33.0	<b>32.3</b>	30.1	32.4	38.5	38.6	<b>38.2</b>	<b>34.3</b>	37.4
Ours	<b>48.7</b>	33.3	26.8	<b>31.2</b>	<b>35.0</b>	<b>49.5</b>	35.6	31.8	33.1	<b>37.5</b>

TABLE VI: Comparison with the state-of-the-art methods under the 1-shot and 5-shot setting. Our proposed network outperforms all previous methods and achieves new state-of-the-art performance. The results reported on PASCAL VOC 2012 dataset with FBIOU(%).

Method	1-shot (%)	5-shot (%)
OSLM [32]	61.3	61.5
co-fcn [39]	60.9	60.2
sg-one [41]	63.1	65.9
R-DFCN [40]	60.9	66.0
PL [33]	61.2	62.3
A-MCG [48]	61.2	62.2
CANet [1]	66.2	69.6
CRNet [2]	66.8	71.5
PFENet [6]	73.3	73.9
Ours	<b>73.5</b>	<b>74.1</b>

TABLE VII: Comparison with the state-of-the-art methods under the 1-shot and 5-shot setting with FSS-1000 dataset. Our proposed network achieves state-of-the-art performance. The results reported with standard mIoU(%).

Method	1-shot	5-shot
OSLSM [32]	70.3	73.0
co-fcn [39]	71.2	74.2
FSS-1000 [38]	73.4	80.1
FOMAML [49]	75.1	80.6
Ours	<b>82.5</b>	<b>83.8</b>

FN denotes false negative,  $n$  denotes the classes' number. The standard mIoU is calculated by averaging the IoU of all classes. The  $IoU_{fg}$  is calculated with equation 9, which only considers the object foreground and ignores the categories, and  $IoU_{bg}$  is calculated in the same way but reversed the foreground and background. FBIOU average the  $IoU_{fg}$  and the  $IoU_{bg}$ .

2) **Dataset: PASCAL VOC 2012.** We validate our methods on the PASCAL VOC 2012 dataset with cross-validation

$$FBIOU = \frac{1}{2}(IoU_{fg} + IoU_{bg}). \quad (11)$$

where TP denotes true positive, FP denotes false positive,



TABLE VIII: Comparison with the state-of-the-art methods under the weakly supervised 1 shot setting. Our proposed network achieves state-of-the-art performance. The results reported on PASCAL VOC 2012 dataset and FSS-1000 dataset with standard mIoU(%).

Method	mIoU(%)	
	PASCAL	FSS-1000
PANet [3] (Bounding box annotations)	45.1	-
CANet [1] (Bounding box annotations)	52.0	-
TeB [50] (Bounding box annotations)	-	78.2
Ours (Bounding box annotations)	<b>55.4</b>	<b>80.8</b>

experiments. Follow OSLSM [32]; we split the 20 object categories into 4 folds, three for training and one for testing. For more details about the dataset information and the evaluation metric, please refer to [32].

**MS COCO and FSS-1000.** The major limitation for PASCAL VOC 2012 is that it contains only a few categories that are not sufficient enough to verify the model’s capabilities on few-shot segmentation tasks. To evaluate our model more fair and effective, we experiment with our model on more complicated datasets containing more categories and images.

MS COCO 2014 [57] is a challenging large-scale dataset that contains 80 categories, 82783 training images, and 40504 validation images. Follow the previous work [6]. We split the 80 object categories into 4 folds, three for training and one for testing.

FSS-1000 [38] introduces a dataset that increases the number of object categories instead of the number of images. In particular, FSS-1000 involves 1000 classes, and each class contains 10 images. Following [38], we choose 520 classes for training, 240 classes for validation and 240 classes for testing.

### B. Implementation Details

Our approach exploits multi-level features from the Resnet50 as our feature representations. We adopt dilated convolution to resolve the feature maps not smaller than 1/8 of the input image. We adopt random flipping, random cropping, random rotation, and random scale as data augmentation during training. We utilize SGD as the optimal to train our network with a cross-entropy loss. The initial learning rate is set to 0.0025, and we adopt a poly-policy decay learning rate with a power equals 0.9.

We train our methods on PASCAL-5<sup>i</sup> dataset for 200 epochs and a batch size 4 with an initial learning rate of 0.0025. For the experiment on MS COCO, our models trained for 50 epochs with a batch size of 32 and an initial learning rate of 0.02. For the experiment on FSS-1000, we set the batch size to 4 and an initial learning rate of 0.0025 to train our model for 100 epochs.

### C. Ablation study

In this section, we inspect how each component affects our network, and we validate the performance of the components

on the PASCAL VOC 2012 dataset. We implement cross-validation experiments at 1-shot setting and report the results with the standard mean IoU. As shown in Table I, we establish the network without any of our proposed components as a baseline. By adding the component one by one, each component can bring a significant performance improvement. In the beginning, we add the message flow module after the CNN encoder, which can improve 1.1 mIoU over the baseline. Our multi-task learning aims to make the network step over the data domain gap; as shown in the table, multi-task training can bring 1.9 mIoU improvement over the baseline. We also adopt the Mask Refinement module proposed in CANet [1], which aims to refine the coarse prediction. In our network, the mask refinement can only bring 0.2 mIoU improvement; we conjecture that our prediction can already cover most of the discriminative object regions, so the mask-refinement module may not determine more object regions. Follow [6]; we generate a prior mask as a rough foreground probability map to guide the final segmentation, which brings a 0.8 mIoU improvement. Our optimal transport module can identify the most confident object regions. As shown in Table I, our partial transport optimal module can bring 0.5 mIoU improvement; combine with other components, our network can total improve 3.4 mIoU over the baseline.

**Inner Flow vs. Cross Flow.** Table II analysis our model message flow module. Both message flow will bring improvement over the baseline. Combine inner, and cross-flow modules will further improve the performances.

**Partial Optimal Matching vs. Full Optimal Matching.** We experiment with a variant by replacing the partial optimal transport with the full optimal transport module to solve the transport problem. As shown in Table III, both partial and full optimal transport modules can bring improvement over the baseline. To investigate how the matching correspondences effect when combining with the prior mask [6], we add our optimal matching correspondences after the prior mask to guide our network. The partial optimal correspondences can improve the performances, but the full optimal correspondences drop the performances. We conjecture that the prior mask locates most of the foreground roughly, and our partial matching correspondences locate the confident foreground areas. However, the full matching correspondences may locate some wrong foreground areas as noise.

### D. Comparison with other state-of-the-art methods

In this section, we compare our network with other state-of-the-art methods on PASCAL VOC 2012 dataset, MS COCO dataset, and FSS-1000 dataset.

**PASCAL VOC 2012.** Table IV and Table VI shows the performance of different methods in both 1-shot and 5-shot setting. We use FBIOU and standard mIoU as the evaluation metric to report our results. The difference between FBIOU and mIoU is that the FBIOU ignores the object category and calculates both foreground and background Intersection-over-Union. We achieve the new state-of-the-art under both 1-shot and 5-shot settings with both FBIOU and mIoU evaluation metrics.



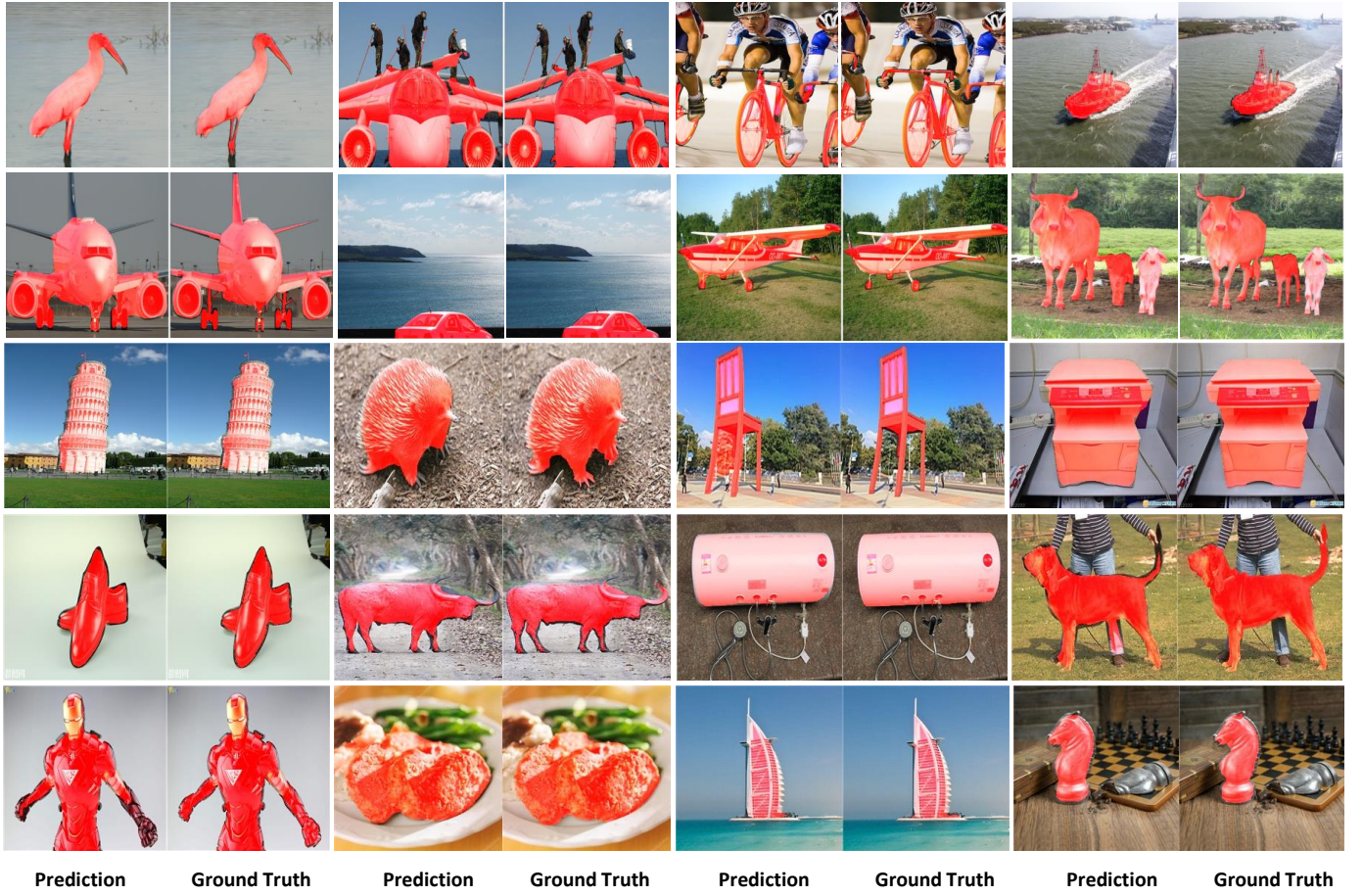


Fig. 5: Our qualitative examples on the PASCAL VOC and FSS-1000 dataset. The first two rows are the results from PASCAL VOC, and the last three rows are the results from FSS-1000. The left column is the prediction, and the right column is the ground truth.

**MS COCO.** As shown in Table V, we cross-evaluate our methods on the dataset MS COCO [57] under both 1-shot and 5-shot setting. Our methods outperform all the previous state-of-the-art methods.

**FSS-1000.** The comparison results with FSS-1000 dataset [38] under both 1-shot and 5-shot setting are shown in Table VII. Our methods outperform all previous methods and achieve new state-of-the-art performance.

#### E. Weakly supervised few shot segmentation

Follow CANet [1] and TeB [50]; we further evaluate our proposed CMNet with a weaker annotation such as bounding boxes. We generate the bounding box annotations from PASCAL VOC 2012, SDS [58], and FSS-1000 [38] dataset by locating every object. During testing, we replace pixel-level annotation with the bounding boxes. As is shown in Table VIII, our CMNet outperforms all the previous methods and achieves new state-of-the-art in both PASCAL VOC 2012 and FSS-1000 datasets under the weakly supervised few-shot segmentation setting.

#### F. Failure case analysis

In this section, we analyze the challenging cases that fail our model. As shown in Figure 6, our model fails to distinguish between the dogs and cats, chairs and tables, cars and buses. This is because they have a similar pattern: difficult to distinguish without semantic information. Moreover, our model can not locate the bird bodies because the query-image only contains the bird's body information lacking semantic information.

#### V. CONCLUSION

This work develops a Correspondences Matching Network for few-shot segmentation. By leveraging a partial optimal transport module and the message flow module, we explore the element-to-element correspondence as the foreground to guide our final prediction. Furthermore, We explore the few-shot segmentation task as a multi-task problem to alleviate the domain gap issue between different datasets. Experiments on PASCAL VOC 2012, MS COCO, FSS-1000 dataset validate our contribution.

#### REFERENCES

- [1] C. Zhang, G. Lin, F. Liu, R. Yao, and C. Shen, "Canet: Class-agnostic segmentation networks with iterative refinement and attentive few-shot



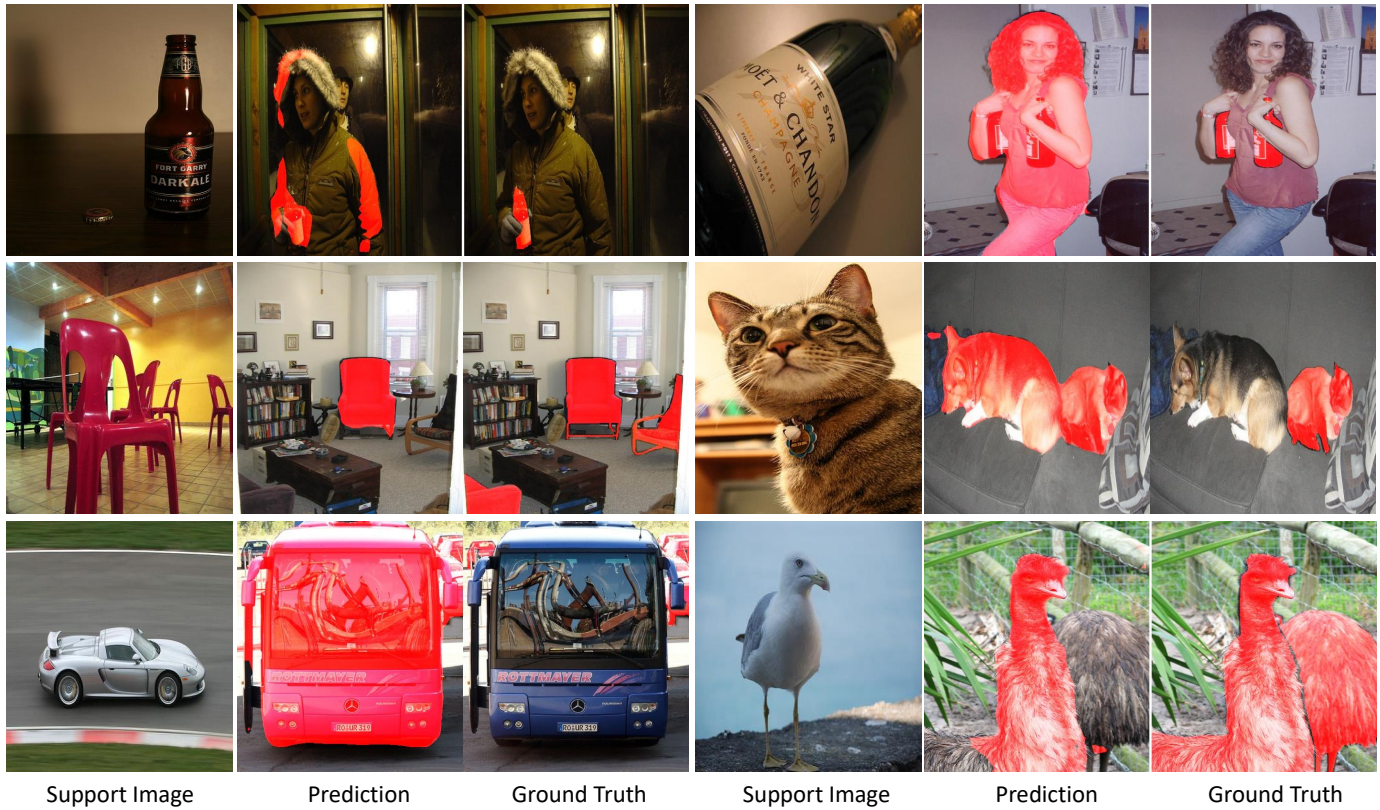


Fig. 6: The failure cases on PASCAL VOC 2012 dataset.

- learning,” in *Proceedings of the IEEE Conference on Computer Vision and Pattern Recognition*, 2019, pp. 5217–5226. 1, 2, 5, 6, 7, 8, 9
- [2] W. Liu, C. Zhang, G. Lin, and F. Liu, “Crnet: Cross-reference networks for few-shot segmentation,” in *Proceedings of the IEEE/CVF Conference on Computer Vision and Pattern Recognition*, 2020, pp. 4165–4173. 1, 2, 5, 6, 7
- [3] K. Wang, J. H. Liew, Y. Zou, D. Zhou, and J. Feng, “Panet: Few-shot image semantic segmentation with prototype alignment,” in *Proceedings of the IEEE International Conference on Computer Vision*, 2019, pp. 9197–9206. 1, 2, 5, 7, 8
- [4] C. Zhang, G. Lin, F. Liu, J. Guo, Q. Wu, and R. Yao, “Pyramid graph networks with connection attentions for region-based one-shot semantic segmentation,” in *Proceedings of the IEEE International Conference on Computer Vision*, 2019, pp. 9587–9595. 2, 6
- [5] H. Wang, X. Zhang, Y. Hu, Y. Yang, X. Cao, and X. Zhen, “Few-shot semantic segmentation with demographic attention networks,” 2, 6
- [6] Z. Tian, H. Zhao, M. Shu, Z. Yang, R. Li, and J. Jia, “Prior guided feature enrichment network for few-shot segmentation,” *IEEE Annals of the History of Computing*, no. 01, pp. 1–1, 2020. 2, 5, 6, 7, 8
- [7] R. Azad, A. R. Fayjie, C. Kauffmann, I. Ben Ayed, M. Pedersoli, and J. Dolz, “On the texture bias for few-shot cnn segmentation,” in *Proceedings of the IEEE/CVF Winter Conference on Applications of Computer Vision*, 2021, pp. 2674–2683. 2
- [8] M. Boudiaf, H. Kervadec, Z. I. Masud, P. Piantanida, I. Ben Ayed, and J. Dolz, “Few-shot segmentation without meta-learning: A good transductive inference is all you need?” in *Proceedings of the IEEE/CVF Conference on Computer Vision and Pattern Recognition*, 2021, pp. 13 979–13 988. 2
- [9] B. Zhang, J. Xiao, and T. Qin, “Self-guided and cross-guided learning for few-shot segmentation,” in *Proceedings of the IEEE/CVF Conference on Computer Vision and Pattern Recognition*, 2021, pp. 8312–8321. 2
- [10] G. Li, V. Jampani, L. Sevilla-Lara, D. Sun, J. Kim, and J. Kim, “Adaptive prototype learning and allocation for few-shot segmentation,” in *Proceedings of the IEEE/CVF Conference on Computer Vision and Pattern Recognition*, 2021, pp. 8334–8343. 2
- [11] J. Deng, W. Dong, R. Socher, L.-J. Li, K. Li, and L. Fei-Fei, “Imagenet: A large-scale hierarchical image database,” in *CVPR*, 2009, pp. 248–255. 2, 6
- [12] J. Long, E. Shelhamer, and T. Darrell, “Fully convolutional networks for semantic segmentation,” in *Proceedings of the IEEE conference on computer vision and pattern recognition*, 2015, pp. 3431–3440. 2
- [13] G. Lin, F. Liu, A. Milan, C. Shen, and I. Reid, “Refinenet: Multi-path refinement networks for dense prediction,” *IEEE transactions on pattern analysis and machine intelligence*, vol. 42, no. 5, pp. 1228–1242, 2019. 2
- [14] L.-C. Chen, G. Papandreou, I. Kokkinos, K. Murphy, and A. L. Yuille, “Deeplab: Semantic image segmentation with deep convolutional nets, atrous convolution, and fully connected crfs,” *IEEE transactions on pattern analysis and machine intelligence*, vol. 40, no. 4, pp. 834–848, 2018. 2
- [15] H. Ding, X. Jiang, B. Shuai, A. Q. Liu, and G. Wang, “Semantic segmentation with context encoding and multi-path decoding,” *IEEE Transactions on Image Processing*, vol. 29, pp. 3520–3533, 2020. 2
- [16] B. Kang, Y. Lee, and T. Q. Nguyen, “Depth-adaptive deep neural network for semantic segmentation,” *IEEE Transactions on Multimedia*, vol. 20, no. 9, pp. 2478–2490, 2018. 2
- [17] H. Shi, H. Li, F. Meng, Q. Wu, L. Xu, and K. N. Ngan, “Hierarchical parsing net: Semantic scene parsing from global scene to objects,” *IEEE Transactions on Multimedia*, vol. 20, no. 10, pp. 2670–2682, 2018. 2
- [18] T. Zhang, G. Lin, J. Cai, T. Shen, C. Shen, and A. C. Kot, “Decoupled spatial neural attention for weakly supervised semantic segmentation,” *IEEE Transactions on Multimedia*, vol. 21, no. 11, pp. 2930–2941, 2019. 2
- [19] H. Shi, H. Li, Q. Wu, and K. N. Ngan, “Query reconstruction network for referring expression image segmentation,” *IEEE Transactions on Multimedia*, vol. 23, pp. 995–1007, 2020. 2
- [20] L. Zhou, C. Gong, Z. Liu, and K. Fu, “Sal: Selection and attention losses for weakly supervised semantic segmentation,” *IEEE Transactions on Multimedia*, vol. 23, pp. 1035–1048, 2020. 2
- [21] W. Liu, G. Lin, T. Zhang, and Z. Liu, “Guided co-segmentation network for fast video object segmentation,” *IEEE Transactions on Circuits and Systems for Video Technology*, 2020. 2
- [22] W. Liu, C. Zhang, G. Lin, T.-Y. Hung, and C. Miao, “Weakly supervised segmentation with maximum bipartite graph matching,” in *Proceedings*

- of the 28th ACM International Conference on Multimedia, 2020, pp. 2085–2094. 2
- [23] W. Liu, X. Kong, T.-Y. Hung, and G. Lin, “Cross-image region mining with region prototypical network for weakly supervised segmentation,” 2021. 2
- [24] W. Liu, Z. Wu, H. Ding, F. Liu, J. Lin, and G. Lin, “Few-shot segmentation with global and local contrastive learning,” *arXiv preprint arXiv:2108.05293*, 2021. 2
- [25] T. Zhang, G. Lin, W. Liu, J. Cai, and A. Kot, “Splitting vs. merging: Mining object regions with discrepancy and intersection loss for weakly supervised semantic segmentation,” in *Computer Vision—ECCV 2020: 16th European Conference, Glasgow, UK, August 23–28, 2020, Proceedings, Part XXII 16*. Springer International Publishing, 2020, pp. 663–679. 2
- [26] C. Zhang, N. Song, G. Lin, Y. Zheng, P. Pan, and Y. Xu, “Few-shot incremental learning with continually evolved classifiers,” in *Proceedings of the IEEE/CVF Conference on Computer Vision and Pattern Recognition (CVPR)*, June 2021, pp. 12 455–12 464. 2
- [27] C. Zhang, Y. Cai, G. Lin, and C. Shen, “Deepemd: Few-shot image classification with differentiable earth mover’s distance and structured classifiers,” in *CVPR*, 2019. 2
- [28] —, “Deepemd: Differentiable earth mover’s distance for few-shot learning,” *arXiv e-prints*, 2020. 2
- [29] C. Zhang, G. Li, G. Lin, Q. Wu, and R. Yao, “Cyclesegnet: Object co-segmentation with cycle refinement and region correspondence,” *IEEE Transactions on Image Processing*, 2021. 2
- [30] C. Zhang, H. Ding, G. Lin, R. Li, C. Wang, and C. Shen, “Meta navigator: Search for a good adaptation policy for few-shot learning,” in *IEEE International Conference on Computer Vision (ICCV)*, 2021. 2
- [31] X. Sun, Z. Yang, C. Zhang, G. Peng, and K.-V. Ling, “Conditional gaussian distribution learning for open set recognition,” 2020. 2
- [32] A. Shaban, S. Bansal, Z. Liu, I. Essa, and B. Boots, “One-shot learning for semantic segmentation,” *arXiv preprint arXiv:1709.03410*, 2017. 2, 6, 7, 8
- [33] N. Dong and E. Xing, “Few-shot semantic segmentation with prototype learning,” in *BMVC*, 2018. 2, 6, 7
- [34] M. Cuturi, “Sinkhorn distances: Lightspeed computation of optimal transport,” in *Advances in neural information processing systems*, 2013, pp. 2292–2300. 3, 5
- [35] N. Courty, R. Flamary, D. Tuia, and A. Rakotomamonjy, “Optimal transport for domain adaptation,” *IEEE transactions on pattern analysis and machine intelligence*, vol. 39, no. 9, pp. 1853–1865, 2016. 3
- [36] Z. Su, Y. Wang, R. Shi, W. Zeng, J. Sun, F. Luo, and X. Gu, “Optimal mass transport for shape matching and comparison,” *IEEE transactions on pattern analysis and machine intelligence*, vol. 37, no. 11, pp. 2246–2259, 2015. 3
- [37] Q. Zhao, Z. Yang, and H. Tao, “Differential earth mover’s distance with its applications to visual tracking,” *IEEE Transactions on Pattern Analysis and Machine Intelligence*, vol. 32, no. 2, pp. 274–287, 2008. 3
- [38] X. Li, T. Wei, Y. P. Chen, Y.-W. Tai, and C.-K. Tang, “Fss-1000: A 1000-class dataset for few-shot segmentation,” in *Proceedings of the IEEE/CVF Conference on Computer Vision and Pattern Recognition*, 2020, pp. 2869–2878. 6, 7, 8, 9
- [39] K. Rakelly, E. Shelhamer, T. Darrell, A. Efros, and S. Levine, “Conditional networks for few-shot semantic segmentation,” in *ICLR Workshop*, 2018. 7
- [40] M. Siam and B. Oreshkin, “Adaptive masked weight imprinting for few-shot segmentation,” *arXiv preprint arXiv:1902.11123*, 2019. 7
- [41] X. Zhang, Y. Wei, Y. Yang, and T. Huang, “Sg-one: Similarity guidance network for one-shot semantic segmentation,” *arXiv preprint arXiv:1810.09091*, 2018. 7
- [42] M. Siam, B. N. Oreshkin, and M. Jagersand, “Amp: Adaptive masked proxies for few-shot segmentation,” in *Proceedings of the IEEE International Conference on Computer Vision*, 2019, pp. 5249–5258. 7
- [43] K. Nguyen and S. Todorovic, “Feature weighting and boosting for few-shot segmentation,” in *Proceedings of the IEEE International Conference on Computer Vision*, 2019, pp. 622–631. 7
- [44] Z. Dong, R. Zhang, X. Shao, and H. Zhou, “Multi-scale discriminative location-aware network for few-shot semantic segmentation,” in *2019 IEEE 43rd Annual Computer Software and Applications Conference (COMPSAC)*, vol. 2. IEEE, 2019, pp. 42–47. 7
- [45] G. Yang, D. Niu, C. Zhang, and X. Zhao, “Recognizing novel patterns via adversarial learning for one-shot semantic segmentation,” *Information Sciences*, vol. 518, pp. 225–237, 2020. 7
- [46] B. Yang, C. Liu, B. Li, J. Jiao, and Q. Ye, “Prototype mixture models for few-shot semantic segmentation,” *arXiv preprint arXiv:2008.03898*, 2020. 7
- [47] Y. Liu, X. Zhang, S. Zhang, and X. He, “Part-aware prototype network for few-shot semantic segmentation,” in *European Conference on Computer Vision*. Springer, 2020, pp. 142–158. 7
- [48] T. Hu, P. Yang, C. Zhang, G. Yu, Y. Mu, and C. G. Snoek, “Attention-based multi-context guiding for few-shot semantic segmentation,” 2019. 7
- [49] S. M. Hendryx, A. B. Leach, P. D. Hein, and C. T. Morrison, “Meta-learning initializations for image segmentation,” *arXiv preprint arXiv:1912.06290*, 2019. 7
- [50] A. R. Feyjje, R. Azad, M. Pedersoli, C. Kauffman, I. B. Ayed, and J. Dolz, “Semi-supervised few-shot learning for medical image segmentation,” *arXiv preprint arXiv:2003.08462*, 2020. 8, 9
- [51] J.-B. Cordonnier, A. Loukas, and M. Jaggi, “On the relationship between self-attention and convolutional layers,” *arXiv preprint arXiv:1911.03584*, 2019. 5
- [52] P. J. Mucha, T. Richardson, K. Macon, M. A. Porter, and J.-P. Onnela, “Community structure in time-dependent, multiscale, and multiplex networks,” *science*, vol. 328, no. 5980, pp. 876–878, 2010. 5
- [53] V. Nicosia, G. Bianconi, V. Latora, and M. Barthelemy, “Growing multiplex networks,” *Physical review letters*, vol. 111, no. 5, p. 058701, 2013. 5
- [54] J. Gilmer, S. S. Schoenholz, P. F. Riley, O. Vinyals, and G. E. Dahl, “Neural message passing for quantum chemistry,” *arXiv preprint arXiv:1704.01212*, 2017. 5
- [55] P. W. Battaglia, J. B. Hamrick, V. Bapst, A. Sanchez-Gonzalez, V. Zambaldi, M. Malinowski, A. Tacchetti, D. Raposo, A. Santoro, R. Faulkner et al., “Relational inductive biases, deep learning, and graph networks,” *arXiv preprint arXiv:1806.01261*, 2018. 5
- [56] P.-E. Sarlin, D. DeTone, T. Malisiewicz, and A. Rabinovich, “Superglue: Learning feature matching with graph neural networks,” in *Proceedings of the IEEE/CVF Conference on Computer Vision and Pattern Recognition*, 2020, pp. 4938–4947. 6
- [57] T.-Y. Lin, M. Maire, S. Belongie, J. Hays, P. Perona, D. Ramanan, P. Dollár, and C. L. Zitnick, “Microsoft coco: Common objects in context,” in *ECCV*, 2014, pp. 740–755. 8, 9
- [58] B. Hariharan, P. Arbeláez, R. Girshick, and J. Malik, “Simultaneous detection and segmentation,” in *European Conference on Computer Vision*. Springer, 2014, pp. 297–312. 9